

TECHNICAL UNIVERSITY OF DENMARK



46115 Turbulence Modeling, Fall 2024

---

ASSIGNMENT 2

Janne W.S. Jacobs,	s244050
Nicola Quaia,	s232439
Gheorghi Battchiev	s233119

December 9, 2024

# Introduction

This report analyses the fluid flow over a smooth cylinder and relatively vortex shedding at a Reynolds number of 3900. This value of  $Re$  is in the transitional regime range, so the inlet flow can be considered laminar and the perturbation of the cylinder allows to create turbulent eddies that are shed periodically along the wake of the cylinder [1].

Two different categories of turbulence models will be used: Reynolds-averaged Navier–Stokes (RANS) modeling and Large Eddy Simulation (LES) modeling. For each modelling approach, two models are presented:  $k - \epsilon$  and  $k - \omega$  for the RANS and k-equation and Smagorinsky for the LES. Additionally, a turbulent inflow with Turbulent Intensity of 2%, generated through a Divergence-Free Synthetic Eddy Method (DFSEM) is proposed for the LES models. SI units are used everywhere.

A summary of the developed models and relative mesh size are presented in Table 1.

Table 1: Mesh summary for the various simulations. T.I. = Turbulence Intensity in front of the cylinder.

Name	Model	T.I. [%]	Grid size	Number of cells
RANS-keps	$k \epsilon$	0	228 x 84 x 1	23 296
RANS-komega	$k \omega SST$	0	228 x 84 x 1	23 296
RANS-coarse	$k \epsilon$	0	182 x 66 x 1	14 608
RANS-finer	$k \epsilon$	0	274 x 102 x 1	46 080
LES-keq	k - equation	0	648 x 84 x 14	2 529 800
LES-keqTurb	k - equation DFSEM	2	648 x 84 x 14	2 529 800
LES-sma	Smagorinsky	0	648 x 84 x 14	2 529 800
LES-smaTurb	Smagorinsky DFSEM	2	648 x 84 x 14	2 529 800

## A. Summary of References

This technical report includes a brief summary of an online article [2] and a published paper [1]. These summaries serve as an extended introduction and provide a basis for subsequent comparison, aiding in evaluating the accuracy and reliability of our findings.

### A.1. CFD Modeling of Flow Over a Cylinder

This online article [2] treats the CFD modeling of flow over a circular smooth cylinder at different Reynolds numbers. The CFD simulations are run using the ANSYS software. The article introduces governing equation, the standard  $k-\epsilon$  model and its initial and boundary conditions. Furthermore, the settings of the ANSYS program are given.

A grid independence study is performed by comparing the velocity fields of three meshes with different fineness. The lift coefficient and velocity distribution for laminar and turbulent flows are given and compared. At turbulent Reynolds number  $Re = 2902$ , the flow has an asymmetric wake with vortex shedding, the wake region is large compared to the laminar flow, and the separation angle is  $120^\circ$ . The largest  $y^+$  value at the cylinder wall is  $y_{max}^+ \approx 1.9$ .

### A.2. LES of Flow past Circular Cylinder at $Re = 3900$

This paper [1] performs Large Eddy Simulations using to calculate mean and turbulence quantities of flow past a circular cylinder in the lower subcritical regime ( $Re = 3900$ ). It compares the LES settings (domain size, number of grid points, SGS model, numerical procedure and discretisation scheme,  $C_s$  and  $N_c$ ) from past papers with their own settings and then compares the results. The results include mean flow quantities such as mean cylinder drag coefficient  $\overline{C_d}$ , mean base pressure  $\overline{C_{pb}}$ , and separation angle  $\theta_{sep}$  and minimum grid filtered velocity  $\overline{U_{min}}$ . Furthermore, the results include plots of non-dimensionalized centerline and mean filtered velocity ( $U/U_\infty$  and  $U_{CL}/U_\infty$ ) for different  $x$ - and  $y$ -locations. The paper argues that the LES predictions compare reasonably well with measurement

data, but less so in the far wake, where results are influenced by the coarser grid size. The effect of subgrid-scale (SGS) model has a small influence on the overall results.

## B. Full Simulation Set-up

The simulation set-up is based on the OpenFOAM tutorial `basic/potentialFoam/cylinder`, which showcases potential flow past a cylinder. From this, the mesh has been adapted, (see subsection B.1), and the solver application has been changed to `pimpleFoam` for its ability to solve transient turbulent flow. The flow is considered to be incompressible. The initial conditions are presented in subsection B.2. The solver settings from `fvSolution` and `fvSchemes` are similarly copied from appropriate RANS and LES tutorials. The time-stepping scheme has been changed to `CrankNicolson 0.9` for increased accuracy, but with the relaxation factor to keep Euler's stability.

### B.1. Mesh Generation

The mesh has been modified as illustrated in Figure 1. Specifically, the mesh was extended downstream of the cylinder by incorporating blocks 10 and 11. Additionally, the entire domain was meshed to include blocks 12 to 23 on the lower side, which are symmetrical to the blocks on the upper side. Simulating the full mesh was chosen to enhance the reliability of the results, despite the increased computational cost and simulation time. Notably, the full mesh was directly defined in the `BlockMeshDict` file, rather than using the built-in `mirrorMesh` function, to avoid potential boundary issues along the symmetry plane ( $y=0$ ).

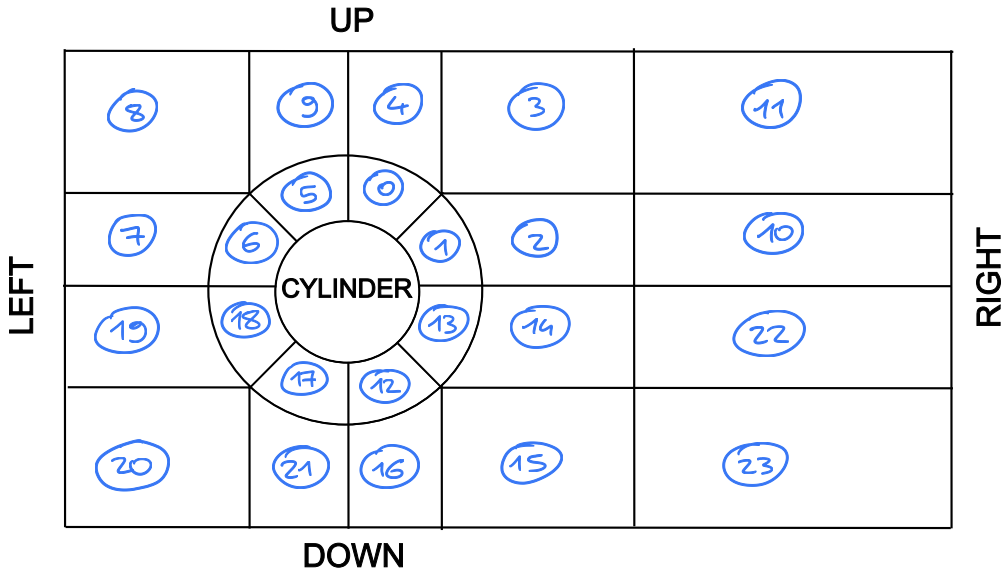


Figure 1: Schematic of flow domain. Numbers indicate the index of the cell blocks. Text indicates boundary patches. Positive  $x$ -direction towards right, positive  $y$ -direction towards up. Right-handed coordinate system.

#### B.1.1. Types of Patches

The types of boundary patches are also shown in Figure 1. The patches `left` and `right` have type `patch` and are considered the flow inlet and outlet respectively. The slip boundary patches `up` and `down` are type `symmetry`. The patch `cylinder` is type `wall` and is considered a no-slip wall. Additionally, the front and back side are `defaultFaces` with `empty` variable values for RANS and are considered `frontAndBack` with type `symmetry` for LES.

This mesh simulates the flow past a cylinder without any physical objects constraining it. Most of the external faces are defined as symmetry planes, though they could alternatively have been defined as patches with a `zeroGradient` condition to better represent boundaries that do not influence the flow. However, using symmetry on a flat plane does not impose any constraints on the flow, making

it a standard practice for modeling slip planes. Consequently, this approach was also adopted for this report.

### B.1.2. Wall-Resolved Flow and Near Wall Cell Size Bounds

The flow will be wall-resolved, giving the mesh a requirement of  $y^+ = 1$  at the cylinder boundary. Since  $y^+$  is flow dependent, this value cannot be set directly. The number of cells and grading in blocks 0, 1, 5, 6, 12, 13, 17 and 18 must be tweaked after an initial run to get a  $y^+$  close to 1.

For accurate LES, Rezaeiravesh and Liefvendahl (2018) [3] suggest a grid resolution in the streamwise direction of  $10 \leq \Delta x^+ \leq 150$  and on the spanwise direction of  $7 \leq \Delta z^+ \leq 70$ . Additionally, the inner-scaled distance of the first cell center from the wall must in the range  $0.25 \leq \Delta y_w^+ \leq 1.96$ .

The main difference for the LES mesh, compared to the RANS mesh, is that the LES requires a 3D grid, while the RANS simulations are run in a (quasi-)2D grid (1 cell in the  $z$ -direction). The number of cells in the  $z$ -directions should be sufficient that the  $\Delta z^+$  condition expressed above is met.

## B.2. Initial and Boundary Conditions

To run the simulations, the analyzed quantities must be initiated. For each of them, a file reporting the boundary conditions (BS) and the initial conditions (IC) must be defined and inserted in the 0.orig folder. A summary of the analyzed quantities and relative IC's is provided below. In general, the inlet is defined by a `fixedValue`, the outlet as `zeroGradient` and other faces as `symmetry`

- **Velocity,  $U$ :** used in all cases, set at 1 in the  $x$  direction on the inlet, `uniform (1 0 0)`.
- **Pressure,  $p$ :** used in all cases. For an incompressible fluid, the pressure can be initially set as 0 in the outlet and `zeroGradient` in the inlet.
- **Turbulent kinematic viscosity,  $\nu_t$ :** used in all cases, set as a very small value to avoid numerical error, `uniform 1e-5`.
- **Turbulence kinetic energy (TKE),  $k$ :** used in the RANS and in the LES-keq model, and not computed for the Smagorinsky model. Set at 0 in the inlet and on the cylinder.
- **TKE dissipation rate,  $\epsilon$ :** applicable for  $k-\epsilon$  model, see subsection C.1. The inlet flow is considered laminar, so  $\epsilon$  is set at a very small value in the left face. As the cylinder is effecting the flow, the value is set to 14.855, taking the value from the `incompressible/pimpleFoam/RAS/pitzDaily` tutorial.
- **Turbulence specific dissipation rate,  $\omega$ :** applicable for  $k-\omega$  model, see subsection C.1. It has an inflow rate of `uniform 300`.

### B.2.1. Reynolds Number

As mentioned before, the velocity inflow has been set with velocity magnitude  $|U| = 1$  m/s. Similarly, the characteristic length, the diameter of the cylinder, is set as  $D = 1$  m. To impose a Reynolds number  $Re = 3900$  the kinematic viscosity  $\nu$  has been set to Equation 1:

$$\nu = \frac{UD}{Re} = 2.5641e-4 \text{ m}^2/\text{s} \quad (1)$$

### B.2.2. Postprocessing tools

For postprocessing purpose, various function are added in the `controlDict` file to save additional simulated quantities, like the `yPlus` field, the Courant Number, the Wall Shear Stress, as well as the force coefficients and the pressure field. Additionally, to compare the results with [1] the field average for  $U$ ,  $p$ , Wall Shear Stress and  $k$  (except for LES-smago) is computed for the mean and fluctuating component, starting after the transient phase. Moreover the LES simulations with 2% turbulence intensity at the inlet produce the velocity field recorded at three probe locations. These probes are positioned at  $x = -1.5$  and  $y = -2, 0$  and  $2$ .

## C. Reynolds-Averaged Navier–Stokes Modeling

Reynolds was a cool guy. Reynolds-Averaged Navier-Stokes (RANS) modeling is a computationally efficient method for predicting mean flow characteristics and key turbulence quantities, such as turbulence kinetic energy (TKE). This approach simplifies the computational demands compared to more detailed turbulence models. The standard  $k-\epsilon$  model and the  $k-\omega$  Shear Stress Transport model will be used for simulations.

### C.1. Standard $k-\epsilon$ vs. $k-\omega$ Shear Stress Transport Model

The standard  $k-\epsilon$  model is a 2-equation RANS model, using the TKE and TKE dissipation rate. This model has been shown to be useful in flow with small pressure gradients and free-shear layer flows<sup>1</sup>. The  $k-\omega$  Shear Stress Transport (SST) model is an extension of the  $k-\omega$  model, which uses the TKE and the turbulence specific dissipation rate,  $\omega$ . The  $k-\omega$  SST uses the  $k-\omega$  in the boundary layer, giving it better performances in adverse pressure gradients, separating flow and the viscous sub-layer. In the free stream the model switches to  $k-\epsilon$  behavior. Both models overestimate the TKE at stagnation points, but SST does less so<sup>2</sup>.

### C.2. RANS Results

The instantaneous flow field of velocity magnitude  $|U|$  for the  $k-\epsilon$  and  $k-\omega$  SST simulations are presented for two different times  $t$  in Figure 2 and 3. Figure 2 shows the flow field at  $t = 20$  s. This is nearing the end of the transient phase, and it can be seen that vortices have started forming and shedding. The  $k-\epsilon$  starts this process a few seconds earlier. It can be seen that those vortices are already farther downstream. The  $k-\omega$  SST model is also in a different phase in its shedding, just having formed a downwards vortex. The vortices can be recognized by their local high velocities in red. Figure 3 shows the flow field 'steady' oscillating state. The flow is not steady, but the oscillations are mostly constant in amplitude and period. The  $k-\omega$  SST model has less concentrated velocity gradients, with less extreme peaks than the  $k-\epsilon$  model.

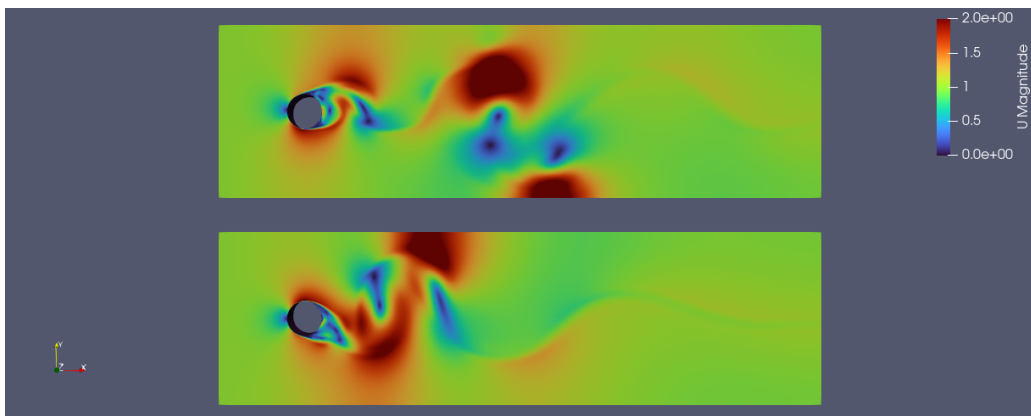


Figure 2: Flow field of velocity magnitude  $|U|$  for  $k-\epsilon$  (upper) and  $k-\omega$  SST (lower) at  $t = 20$  s.

Figure 4 shows the drag and lift coefficients,  $C_D$  and  $C_L$  respectively. It can be seen that in the initial startup ( $t < 30$  s for  $k-\epsilon$  and  $t < 40$  s for  $k-\omega$ ) the system is in a transient phase. After this time, the system is in the 'steady' oscillating state, corresponding to the vortices being shedded with a total of 22 periods which is very much in line to what was done in [1] where 20 periods were used for the calculation for the mean flow quantities.

The drag coefficients are listed in Table 2 in Section F, where they are also compared to the values from the LES simulations and literature. The lift coefficients have a mean value very close to 0 and are oscillating around this. The mean lift coefficient is expected to be zero, as a symmetric shape such as a cylinder should produce no lift.

<sup>1</sup>[https://www.cfd-online.com/Wiki/K-epsilon\\_models](https://www.cfd-online.com/Wiki/K-epsilon_models)

<sup>2</sup>[https://www.cfd-online.com/Wiki/SST\\_k-omega\\_model](https://www.cfd-online.com/Wiki/SST_k-omega_model)

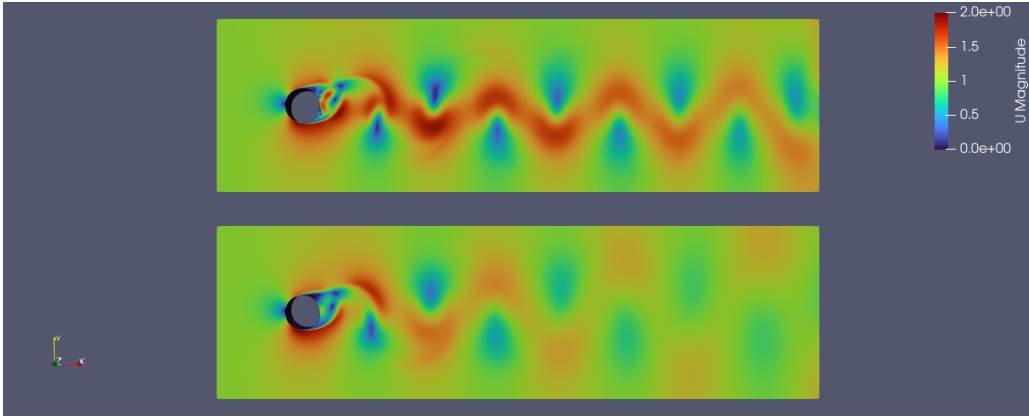


Figure 3: Flow field of velocity magnitude  $|U|$  for  $k-\epsilon$  (top) and  $k-\omega$  SST (bottom) at  $t = 50$  s.

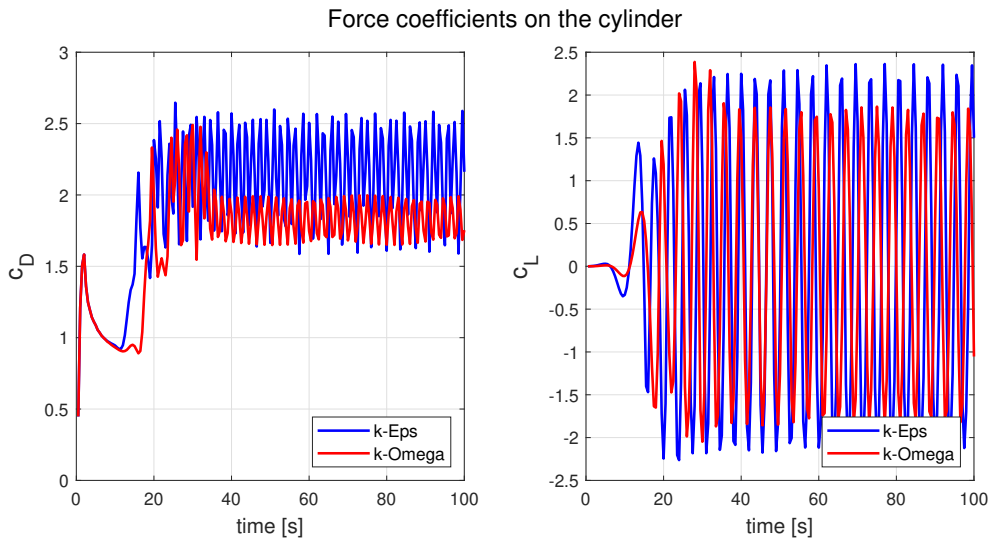


Figure 4: Drag coefficient  $C_D$  and lift coefficient  $C_L$  over time for  $k-\epsilon$  and  $k-\omega$ .

The pitch, roll, and yaw moment coefficients, similarly to the lift coefficient, are expected to be zero. The simulations show values on the order of magnitude of  $1 \times 10^{-3}$ ,  $1 \times 10^{-20}$ , and  $1 \times 10^{-20}$ , respectively.

## D. Large Eddy Simulations

Large Eddy Simulations (LES) place themselves as an intermediate solution approach between the low-fidelity RANS and the high-fidelity high-computational cost of the direct numerical simulations (DNS). In fact, in LES, the contribution in energy and momentum of the large eddies is explicitly computed, while the small-scale turbulence is modeled [4]. Special attention will be given in this report to the ratio between the resolved and modeled flow.

### D.1. Updated Mesh

As mentioned in subsection B.1, a proper LES requires a 3-dimensional mesh. For this reason, the grid along the z direction is divided in 14 cells. This number has been chosen to obtain a  $z^+ \approx 30$ , meaning  $\Delta z \approx 30 \Delta y$ , as  $y^+$  was previously computed to be around 1. Additionally, the new front and back faces are defined in the `blockMeshDict` file (as well as the other input files) as symmetry faces, as it is assumed that they do not interfere with the flow. To ensure sufficient mesh refinement downstream of the cylinder, the number of grid points in the flow direction was increased. Additionally, as for the RANS simulation, the resolution around the cylinder is considered sufficiently high, eliminating the need for a wall function. Two different models are then considered: the Smagorinsky model and the k-equation model, and both are evaluated without and with turbulent inflow at the cylinder inlet.

## D.2. Smagorinsky Model vs k-equation Model

In the Smagorinsky model, the eddy viscosity is directly related to the grid dimension, as can be seen in Equation 2 taken from [5]. In the formula,  $\Delta$  represents a physical dimension related to the grid size. From a practical point of view, applying this model in OpenFoam requires solving for  $U$ ,  $p$  and  $\nu_T$ .

$$\nu_T = C_S \Delta^2 |S| \quad (2)$$

The k-equation model, on the other hand, solves also for the subgrid-scale turbulent kinetic energy ( $k_{SGS}$ ). Hence, this model is more computationally expensive than the Smagorinsky model due to the added transport equation, but it is more flexible, especially in regions with complex flows with strong inhomogeneities [6]. In OpenFoam, a file for  $k$  and relative solution scheme must be added to implement the k-equation model.

## D.3. Resolved ratio

As mentioned before, a very important quantity to evaluate when choosing a correct LES mesh is the ratio between the resolved, meaning actually computed, and the modeled flow. In practise, this can be evaluated following Equation 3, in which  $k_{RES}$  is computed from Equation 4 and  $k_{SGS}$  is the output  $k$  given by the k-equation model. A correct LES should have a ratio of at least 80%.

$$\text{ratio} = \frac{\langle k_{RES} \rangle}{\langle k_{RES} \rangle + \langle k_{SGS} \rangle} \quad (3)$$

$$k_{RES} = 0.5 (\text{UPrime2Mean\_XX} + \text{UPrime2Mean\_YY} + \text{UPrime2Mean\_ZZ}) \quad (4)$$

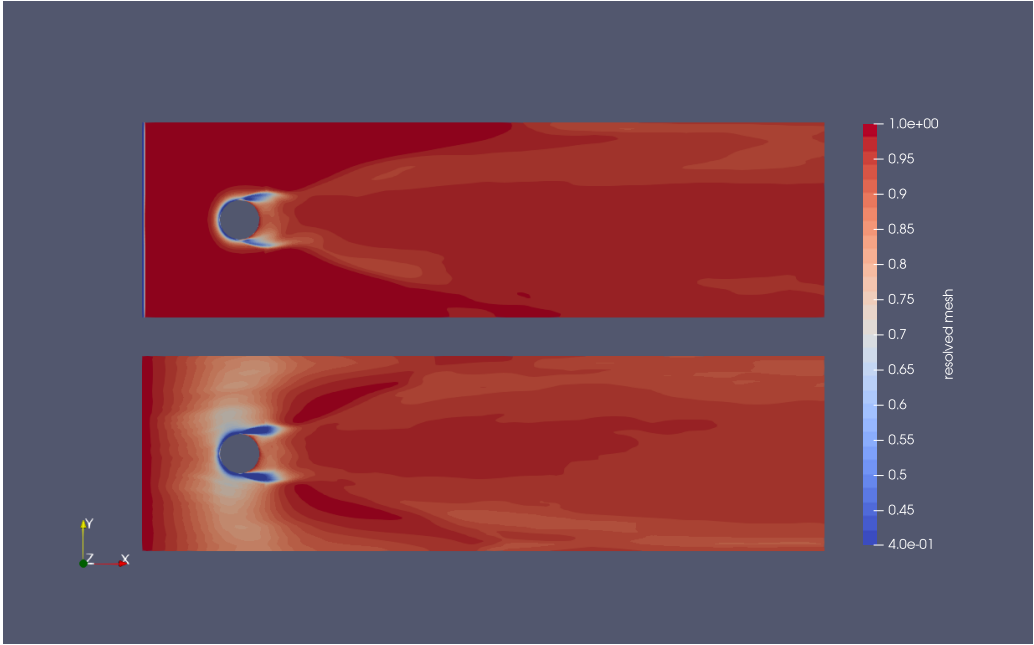


Figure 5: Revolved vs total kinetic energy ratio evaluated for LES k-equation (top) and LES k-equation with 2% turbulent intensity at the cylinder inlet (bottom).

Note that in Equation 3 the quantities are averaged, as the ratio expresses the overall mesh quality and is not dependent on the single turbulent eddy. In practice, these quantities are evaluated by using the function `fieldAverage` to compute the average value of `kmean` and `Uprime2Mean`. The evaluation begins around 20 seconds after the start of the simulation, to allow the transient phase to pass.

Graphically, this ratio is portrayed in Figure 5, for the k-equation model and for the k-equation model with 2% turbulence at the cylinder inlet. For the standard case, the mesh quality is generally adequate, with values remaining above 90% across most of the domain. However, near the cylinder, the ratio drops significantly, reaching nearly zero in the cells closest to the cylinder and approximately 40% at

a distance of  $0.2D$  from the cylinder. Given that the region around the cylinder is where most of the small-scale turbulence is generated, this result can be regarded as a reasonable approximation of the flow characteristics in this area.

#### D.4. LES results

After running the simulation, it was determined that, following the transient phase, the flow exhibits oscillations with a period of approximately 3.6 seconds for the Smagorinsky model and 3.5 seconds for the k-equation model. Due to the high computational cost associated with simulating the finer 3D grid and the LES itself, only 30 seconds of fully developed oscillating flow were modeled, corresponding to roughly six periods. This is in contrast to the 20 periods used in the reference data [1]. Extending the simulation time could have increased the number of periods used to compute the flow statistics, thereby improving overall accuracy.

The two models are compared visually in Figure 6 at 15 seconds, so still in the transient state, and at 30 seconds in Figure 7, where the flow is fully developed and the oscillating behaviour is present. As one can see, the two models are quite similar. As highlighted above, the two wakes are not perfectly in phase, but they are comparable in terms of magnitude and overall behaviour.

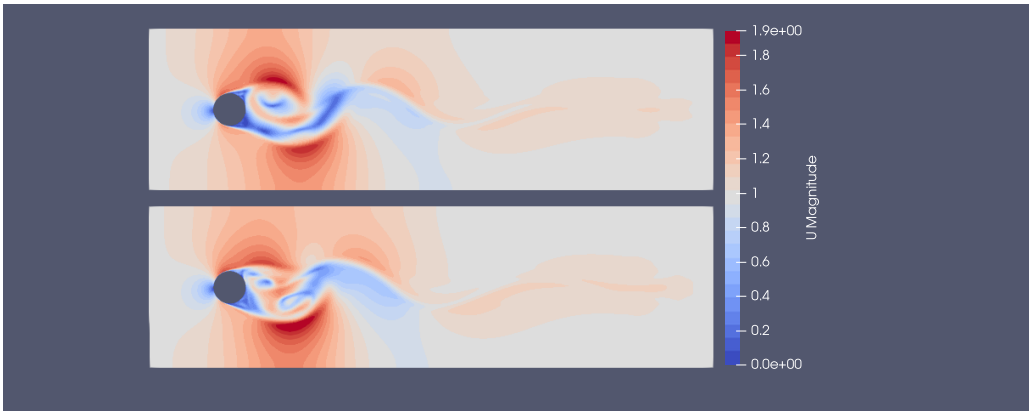


Figure 6: Smagorinsky (top) and k-equation (bottom) models at  $t = 15$  seconds

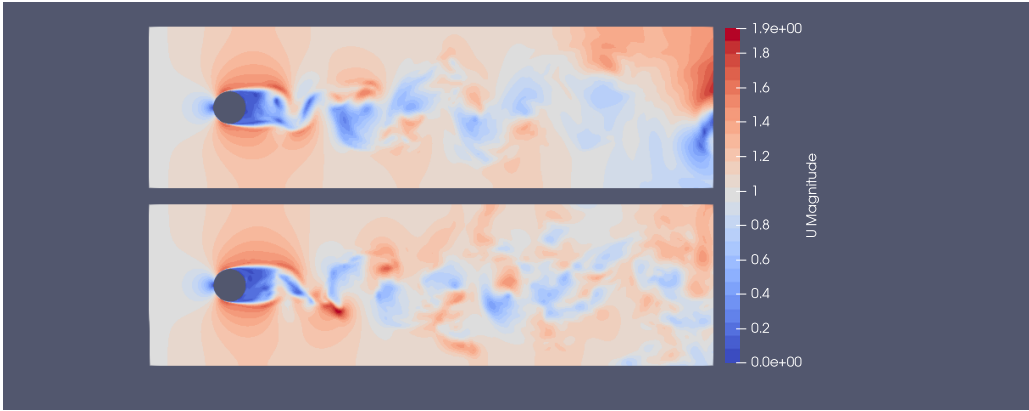


Figure 7: Smagorinsky (top) and k-equation (bottom) models at  $t = 30$  seconds

### E. Turbulent Inlet using Divergence-Free Synthetic Eddy Method (DFSEM)

To generate a turbulent inflow, the inlet condition of the velocity is changed to 'turbulentDFSEMInlet', which simulates a Divergence-Free Synthetic Eddy based on given U (velocity field), R (Reynold stresses), and L (eddy length scale). Additionally, the velocity type of the output (right side) is

changed to 'advective'.

The given U, R, and L files are taken from `/incompressible/pimpleFoam/LES/planefChannel/`. However, these files describe a relatively high turbulent flow in a fully developed, bounded flow, so they need to be modified prior to being applied to the analyzed case study. In particular, from the reference data, the values at larger  $y$  need to be removed, as they are affected by the presence of the wall, and the remaining values should be scaled down to the appropriate turbulence intensity. Two different strategies have been used:

1. **Interpolation:** select the central part of the reference flow, stretch it to the new inlet size, interpolate on the  $y$  position of the centroids of the new mesh
2. **Central value:** extract the value at the center of the flow from the reference, applying it to the new centroids

The resulting input conditions from the original reference, the Interpolation strategy and the Central value strategy are proposed in Figure 8. Note that both strategies have the velocity at a fixed value of 1 m/s to be compliant with the case study. Additionally, both cases have the L and R values scaled by a scaling factor.

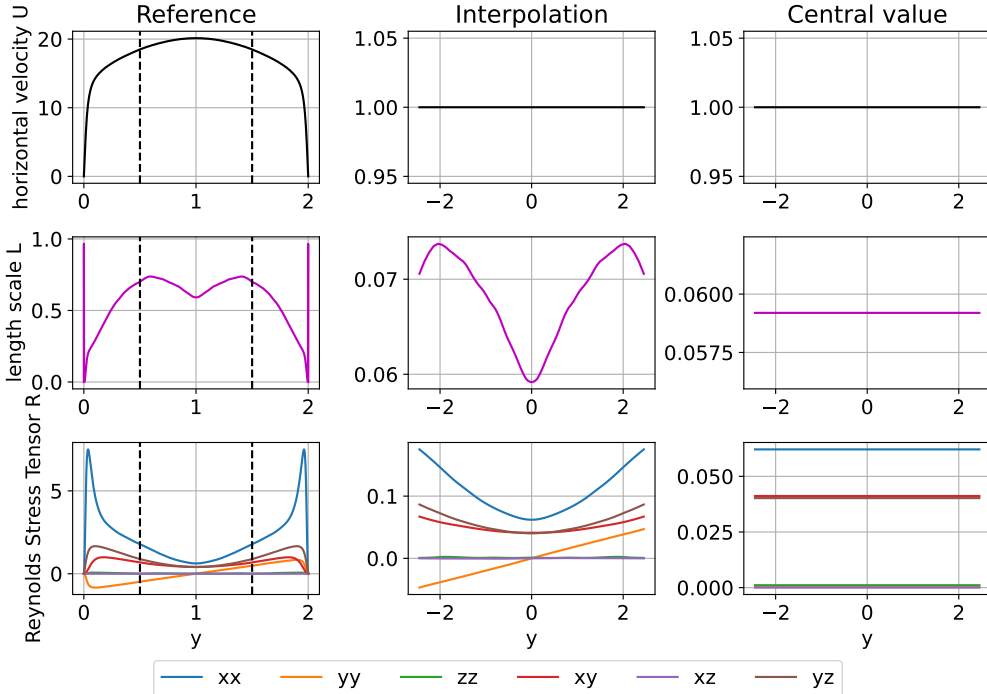


Figure 8: Input data to generate the turbulent inflow for  $U$ ,  $L$   $R$  for the Reference (channel flow), Interpolation and Central value strategy

After running the simulations, 3 probes are positioned at  $x = -1.5$  and  $y = -2, 0$ , and  $2$ , to measure the turbulence intensity of the generated flow. The time history and mean value of the turbulence intensity for the various test cases is portrayed in Figure 9.

As one can see, turbulence intensity is around 2% in both cases. Unfortunately, none of the two strategies allowed to produce a constant turbulence intensity over the  $y$ -direction. Nevertheless, the 'Central value' strategy was chosen as the optimal one, due to its simplicity. The optimal scale factor for the k-equation model is 0.1, while for the Smagorinsky model is 0.11.

Recalling Figure 5, one can notice that the resolved ratio of the turbulent inflow is significantly lower than the one for the laminar inflow. This is due to the added small-scale eddies, that are difficult to correctly capture by the LES method. Additional mesh refinement around the cylinder (blocks 5,0,9,4 and 17,12,21,16) could be used to partially solved the problem.

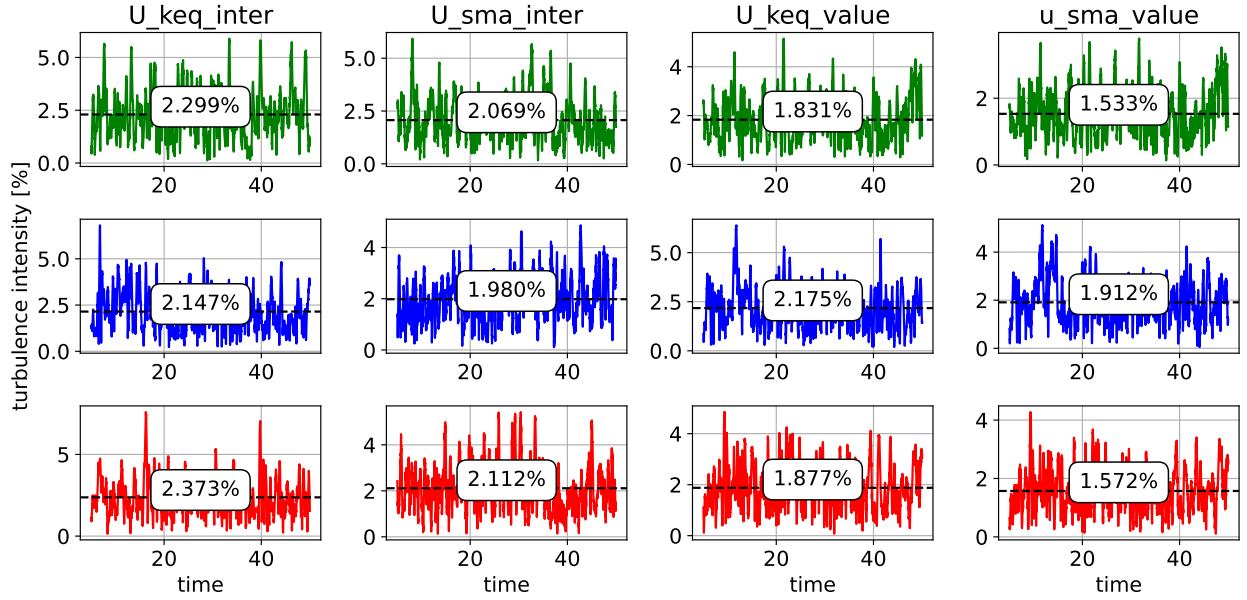
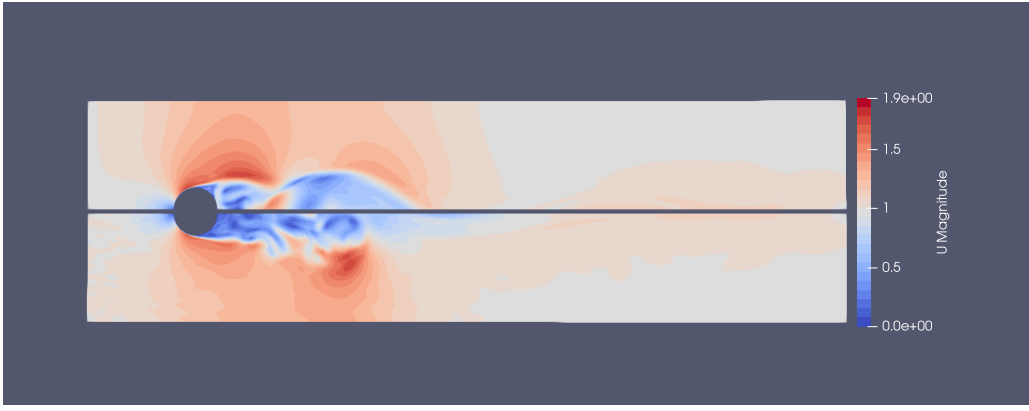


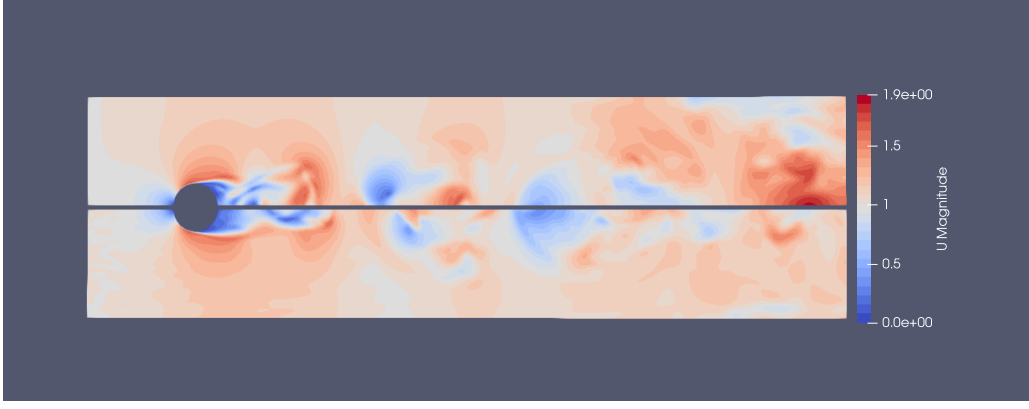
Figure 9: Turbulence intensity measured by the probes positioned at  $x = -1.5$  and  $y = 2$  (green),  $y = 0$  (blue) and  $y = -2.5$  (red). 'inter' stands for the interpolation strategy, while 'value' for constant value strategy

### E.1. Turbulent LES result

The turbulence simulations have a behaviour similar to the laminar inlet case. Visually, laminar and turbulence k-equation model are compared in Figure 10. As one can see, the turbulence affects the wake after the cylinder, reducing the large eddies in smaller eddies. This phenomenon can be noticed in Figure 10a at 15 s, where the eddy just after the cylinder has a 'rougher' profile, and in Figure 10b, where the far wake has a reduced number of eddies. Interestingly, the two simulations have a symmetrical behavior, meaning that the wake of one simulation shifts toward the bottom when the other simulation's wake shifts toward the top, and vice versa. This is likely not related to the presence of turbulence in one of the simulation, but rather due to the stochastic behaviour of the wake formation process that started in one verse in one simulation, and in the other verse in the other.



(a) time = 15 s



(b) time = 30 s

Figure 10: Comparison between the velocity field of the laminar inlet k-equation model (top-half) and turbulent inlet k-equation model (bottom-half) at various time instant.

## F. Verification and Validation of Mesh and Results

In subsection F.2, various statistics from the simulation previously described are compared to each others and to the experimental data from [1] when available. The mesh quality is further analyzed, and a mesh sensitivity study is presented in subsection F.1.

### F.1. Verification of Mesh and Numerical set-up

The quality of the mesh is analyzed by looking at the  $y^+$  values in the wall, presenting the Courant number and by performing a mesh sensitivity study by running a simulation on a coarser and finer mesh.

#### F.1.1. Mesh Sensitivity Study

To perform a mesh sensitivity study, case 1 is run with a coarser mesh ( $n_{\text{cells}} = 14608$ ) that is  $\approx 0.8 \times 0.8 = 0.64 \times$  as fine as the simulation mesh ( $n_{\text{cells}} = 23296$ ), and a finer mesh ( $n_{\text{cells}} = 46080$ ) that is  $\approx 1.4 \times 1.4 = 1.96 \times$  as fine. The following graphs are generated using the  $k - \epsilon$  turbulence model. Both RANS models are based on the same computational mesh. All quantities presented in the graphs are plotted over the upper half of the cylinder, as the results for the lower half are comparable and exhibit similar trends.

As can be seen in Figure 11, the skin friction coefficient over the cylinder changes significantly from the coarse to the simulation mesh. After nearly doubling the number of grid points from the simulation to the finer mesh however, the skin friction shows almost no change, except in moving the bump of  $C_f$  from  $\theta \approx 165^\circ$  to  $\theta \approx 145^\circ$ . Since the change in results is for the most part negligible compared

to the change in cell size, the solution can be considered to be mesh independent for the performed simulation.

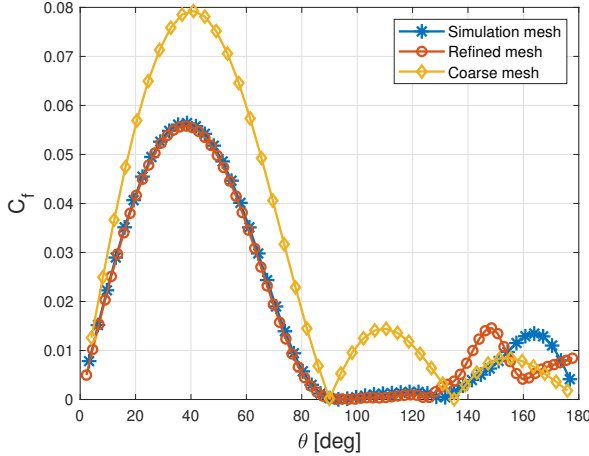


Figure 11: Skin friction coefficient  $C_f$  over the cylinder for three meshes with increasing fineness.

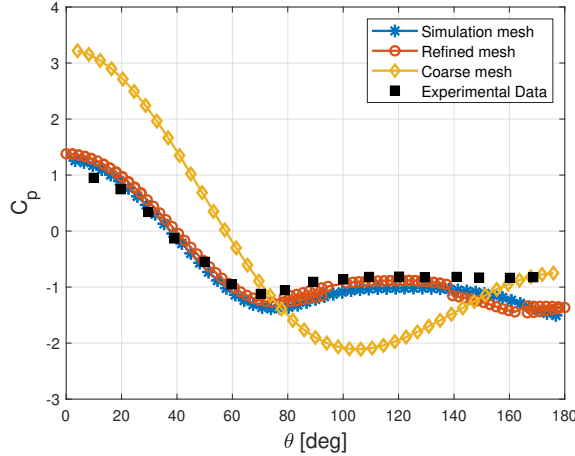


Figure 12: Pressure coefficient  $C_p$  over the cylinder for three meshes with increasing fineness.

It can be noted that will the  $y^+$ -value for the coarse mesh, see Figure 13 is larger than 1 for approximately the first half of the cylinder. However, with  $y^+ < 1.4$  everywhere on the cylinder, the mesh still conforms to the bounds introduced in subsubsection B.1.2 and the  $y^+$ -value is smaller than seen in [1]. This bound and comparison are for LES, but still gives the indication that the mesh is fine enough where wall-resolved flow can be computed. However, the simulation mesh and finer mesh having a maximum  $y^+$  close to 1 and below 1 will obviously be more accurate in this boundary layer region.

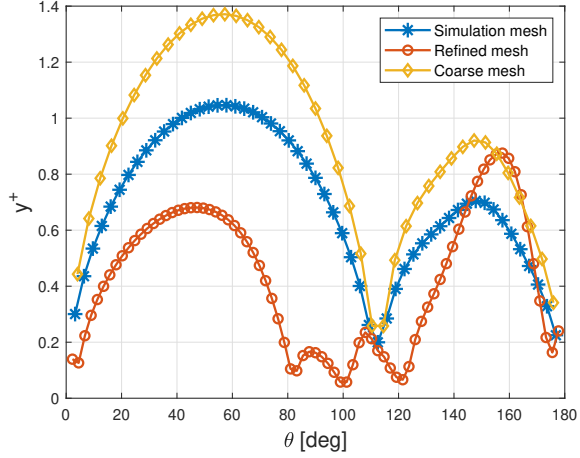


Figure 13:  $y^+$  for the first cell at the cylinder boundary for three meshes with increasing fineness.

### F.1.2. Wall $y$ -plus Values

The  $y^+$  profile on the cylinder as a function of the polar angle is portrayed in Figure 14 for the simulations without turbulent inflow and Figure 15 for all four LES simulations. As a general trend, the  $y^+$  has a low value at  $\theta = 0$ , the stagnation point, as the shear stress is close to 0, as expected. Then the value increases up to  $45^\circ$  for  $k-\epsilon$  and LES k-equation and  $60^\circ$  for  $k-\omega$  SST and LES Smagorinsky, where it reaches its maximum just around 1. In this region the flow has the maximum acceleration, hence the highest shear stresses, hence the highest  $y^+$ . From here the acceleration should decrease to zero at  $\theta = 90^\circ$  where the cylinder contracts the flow the most, decreasing the stresses, until the flow detaches for  $\theta \approx 90^\circ$  for the former two models and around  $\theta = 110^\circ$  for the latter two models. Various models reach different maximum values (0.9 for the  $k-\epsilon$  up to 1.11 for the Smagorinsky) and have different behaviours after the detachment based on their ability to describe the turbulent separation bubble. It can be noticed that there is a similarity between the trend of the k-Omega and Smagorinsky models and between k-eps and k-equation.

Regarding the comparison between laminar inlet and turbulent inlet LES, the turbulence modifies slightly the  $y^+$  behaviour. It changes the Smagorinsky behaviour to be very close to the k-equation. Other than this no more clear trends are visible.

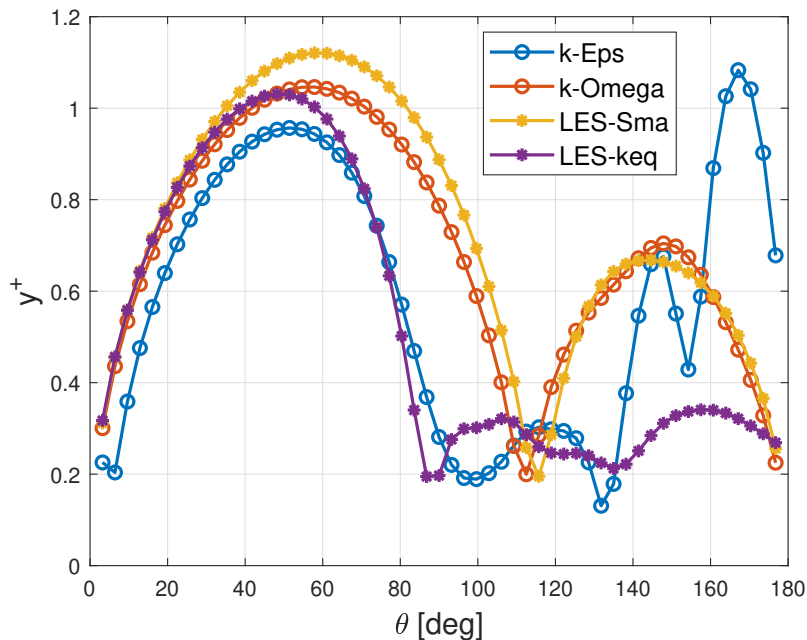


Figure 14: Comparison RANS and LES models:  $y^+$  values over the cylinder.

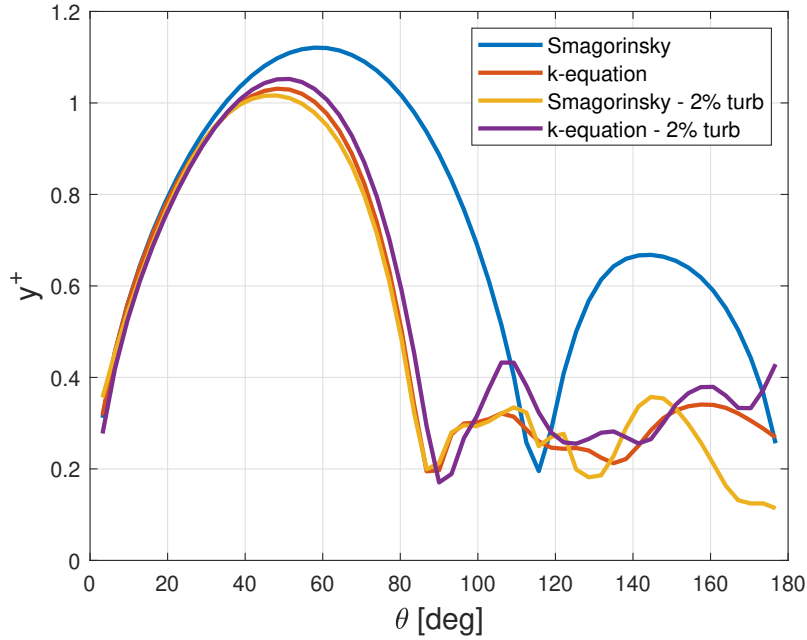


Figure 15: Comparison LES standard models and LES with 2% turbulence intensity at the inlet:  $y^+$  values distributions over the cylinder.

### F.1.3. Courant Number

The Courant number describes how much a fluid particle moves from one time step to the next compared to its cell size. For a reliable and converging simulation, the Courant number must be  $C < 1$ . This is achieved with a time step  $dt = 0.01$  s. In the following figures, the Courant number is shown within the domain for the RANS (Figure 16 and Figure 17) and LES (Figure 18). As the graphs shows, the computed courant is at most 1.1 for RANS and LES, so, for this metric, the mesh can be considered sufficiently refined.

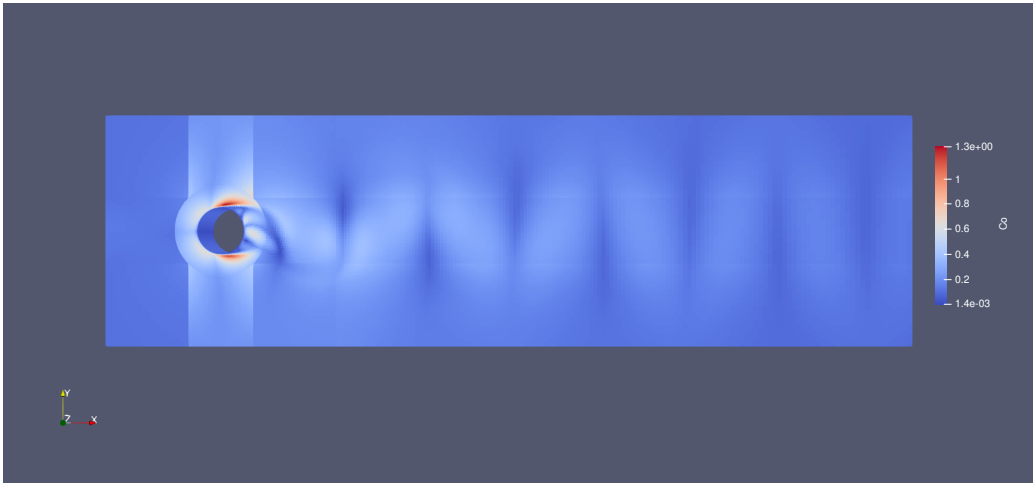


Figure 16: Courant number within the flow domain for RANS  $k-\omega$  SST at  $t = 50$  s.

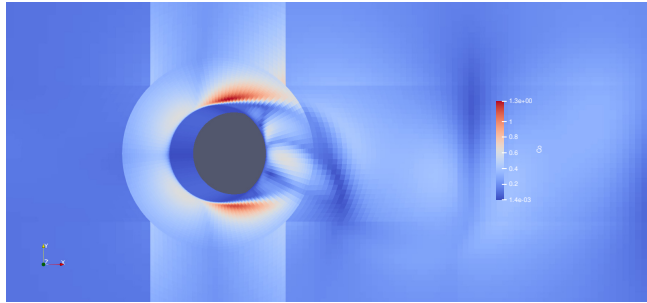


Figure 17: Courant number near the cylinder for RANS  $k$ - $\omega$  SST at  $t = 50$  s.

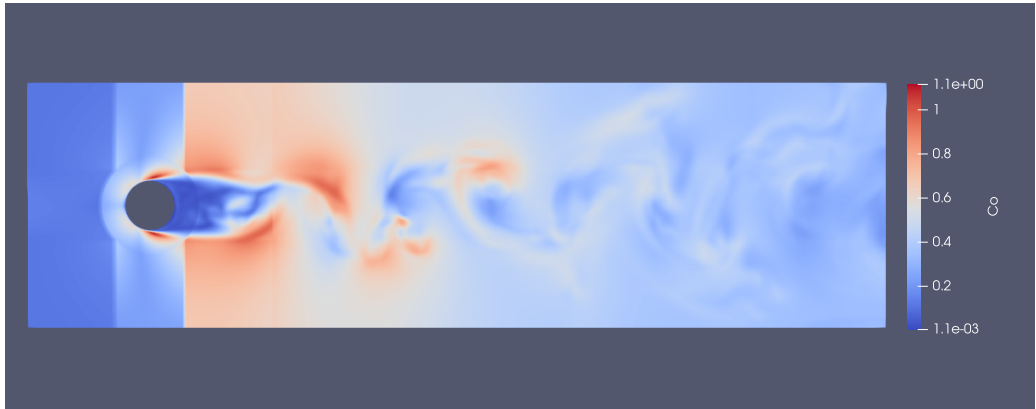


Figure 18: Courant number for the LES  $k$ -equation at  $t = 50$  s.

## F.2. Validation of Results

Firstly, the skin friction coefficient for all simulations are plotted. Then, to validate the results, the pressure and force coefficients and velocity profiles are plotted and compared to not only each other, but experimental data [1] as well.

### F.2.1. Skin Friction

The skin friction can be computed following Equation 5, so it is again dependent on the shear stress  $\tau_w$ , that increases for  $\theta$  between 0 and  $\approx 45 - 60^\circ$ , is reduced until  $90^\circ$ , and then is very dependent on the chosen model.

$$C_f = \frac{\tau_w}{1/2 \rho U^2} \quad (5)$$

Figure 19 compares the skin friction coefficient  $C_f$  from the RANS with the LES. It can be seen that results before separation are very similar. After separation, the RANS models calculate a large increase for  $\theta > 130^\circ$ . This can be explained by RANS's inability to accurately capture the backflow and recirculation in this area.

The LES results stay close to 0 after separation. This can again be seen in Figure 20, where the LES results including the turbulent inflow are compared. It can be seen that again, the influence of the turbulence inflow on the Smagorinsky result is to decrease its difference compared to the  $k$ -equation.

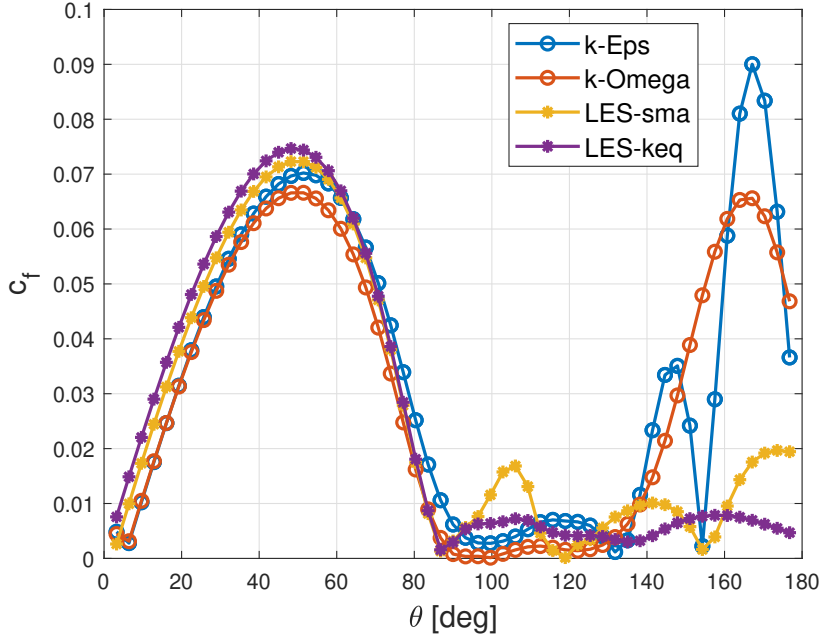


Figure 19: Comparison RANS and LES models: Skin friction coefficient  $C_f$ .

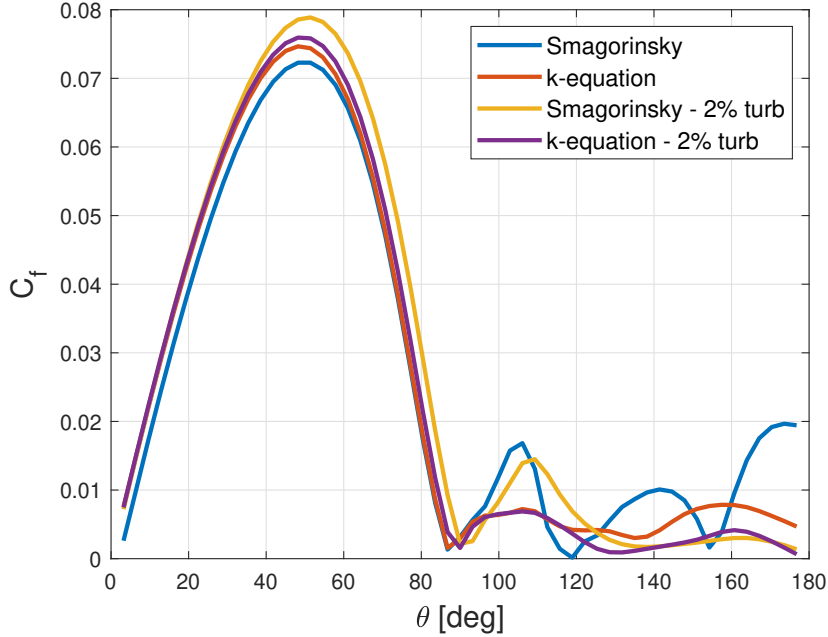


Figure 20: Comparison LES standard models and LES with 2% turbulence intensity at the inlet: Skin friction coefficient  $C_f$ .

### F.2.2. Pressure coefficient

The pressure coefficient  $C_p$  can be calculated as Equation 6. This uses the fact that the atmospheric pressure for incompressible flow can be defined as zero.

$$C_p = \frac{P}{1/2 \rho U_\infty^2} \quad (6)$$

Figure 21 shows the pressure coefficient  $C_p$  over the top half of the cylinder. It can be seen that for  $\theta < 50^\circ$  all models have similar results and very close to the experimental data from *Rajani et al., 2016* [1]. After this angle, the  $C_p$ -profile bends upwards, and the RANS models start to slightly deviate. Both LES models have a near perfect match with each other and the experimental data.

The LES results and experimental data stay constant after the separation, because there is constant pressure in that region<sup>3</sup>. The RANS results dip a small amount below the  $C_p$ , but are still follow the experimental results decently well until  $\theta \approx 120^\circ$ .

Figure 22 plots the pressure coefficient again, but now for comparing the turbulent inlet LES. Again, at the front part of the cylinder ( $\theta < 60^\circ$ ), the pressure coefficient overlap to be nearly identical to each other and the experimental results. The influence of the turbulence inflow seems to increase the accuracy slightly in the constant pressure area, but slightly decrease the accuracy around point, where  $\partial C_p / \partial \theta = 0$ . Overall, due to the already high accuracy, and the partly increased and partly decreased accuracy is hard to say in the turbulence inflow improves the models, but it does show robustness to changing the specified boundary conditions.

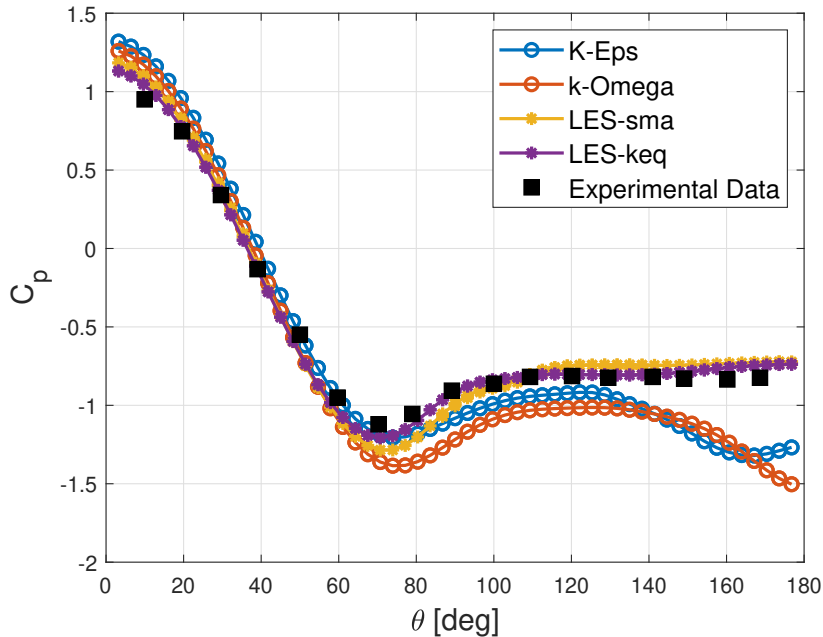


Figure 21: Comparison RANS, LES models and experimental values from [1]: Pressure coefficient over the cylinder

<sup>3</sup><https://www.tec-science.com/mechanics/gases-and-liquids/flow-separation-boundary-layer-separation/>

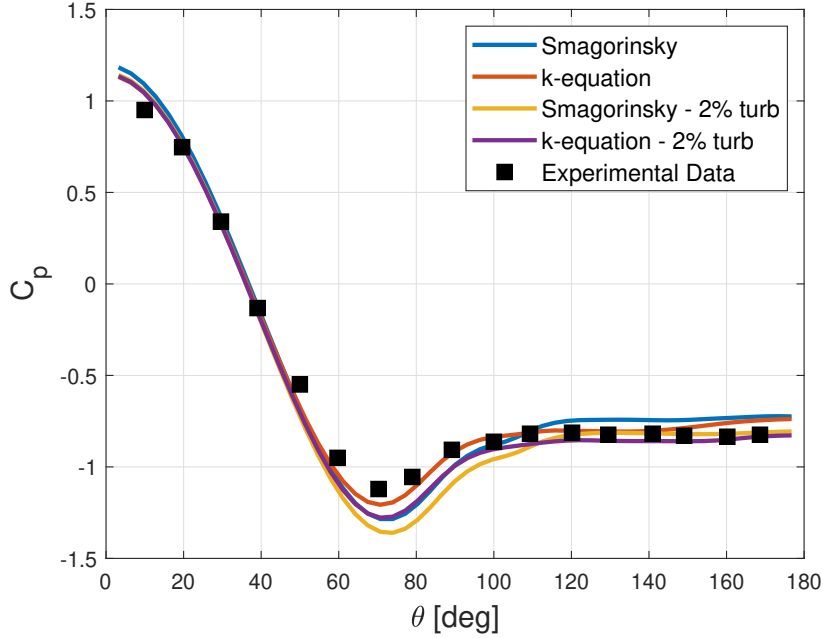


Figure 22: Comparison LES standard models, LES with 2% turbulence intensity at the inlet and experimental values from [1]: Pressure coefficient over the cylinder

### F.2.3. Force Coefficients

To combine the overall flow field results into a single variable, the mean drag coefficient  $\overline{C_D}$  can be used. This variable and the mean lift coefficient  $\overline{C_L}$  are presented for the simulations and two literature sources in Table 2. As mentioned before in subsection C.2, the mean lift coefficient should be zero, and for both RANS and all LES cases they are. The error of the mean error might be decreased if more cycles for the LES are computed.

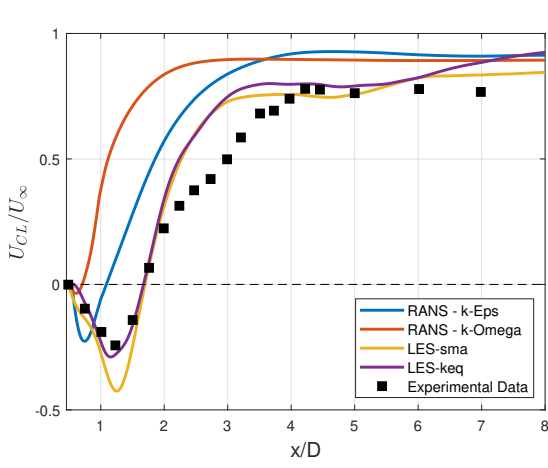
Table 2: Mean drag and lift coefficient  $\overline{C_D}$  and  $\overline{C_L}$ , computed for  $t > 40$  s for 1 and 2,  $t > 20$  s for 3 and 5,  $t > 25$  s for 4 and 6.

Case	$\overline{C_D}$	$\overline{C_L}$
1. RANS $k-\epsilon$ (2D)	1.98	-0.015
2. RANS $k-\omega$ SST (2D)	1.71	0.008
3. LES Smagorinsky	1.23	-0.004
4. LES $k$ -equation	1.22	0.010
5. Smagorinsky with DFSEM	1.28	-0.065
6. $k$ -equation with DFSEM	1.24	-0.083
Measurements from [1]	$0.98 \pm 0.05$	-
Other literature [7]	1.2	-

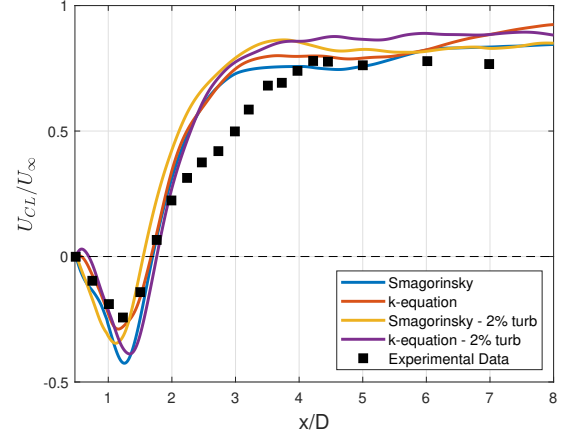
### F.2.4. Mean velocity profiles

First of all, the normalized velocity across the center line is plotted as a function of the normalized centerline in Figure 26a for RANS and LES and in Figure 26b for laminar and turbulent inlet LES, and compared to the experimental data. Note that the x-axis originates at the center of the cylinder, so the first available data is at  $x = 0.5$ . It is possible to notice that the laminar inlet LES are the closest to the experimental data, with  $k$ -equation following the best, especially close to the cylinder wall. This is expected, as  $k$ -equation is the most complex model between the ones used, and it is better in describing regions with complex flow, like the wake just after the cylinder. All models fail to accurately describe the flow far away from the cylinder, and this is coherent with the result presented in [1]. In particular, the less precise is the model (from LES to RANS) the higher is the magnitude of the flow in the center of the domain.

Regarding the turbulent LES (Figure (b)), one can see that the profiles with added turbulence have an higher value of the velocity. This is not because the turbulent flow is faster, but rather because the solution model fails to accurately describe it, and, as seen for the (a) graph, the 'worst' the solution method, the highest is the speed.



(a) Comparison RANS and LES models



(b) Comparison LES standard and LES with 2% turbulence intensity at the inlet

Figure 23: Center line velocity, normalized by freestream velocity,  $U_{CL}/U_\infty$  after the cylinder for normalized distance  $x/D$  for RANS and LES and from [1].

The mean velocities and the components of the Reynolds stress tensor are plotted as a function of  $y/D$  at various distances from the cylinder ( $x/D$ ). The plots are arranged to enable direct comparison with the experimental data presented in [1]. The  $x/D$  values are displayed in descending order as follows:  $x/D = 1.06$ ,  $x/D = 1.54$ ,  $x/D = 2.02$ ,  $x/D = 4$ ,  $x/D = 7$ , and  $x/D = 10$ . For the velocity  $V$ , the plots are shown up to  $x/D = 2.02$ .

As a general trend, LES (Large Eddy Simulation) demonstrates the best agreement with experimental data. Among the models, the Smagorinsky model appears to perform the best across the entire domain. However, deviations from the experimental data are noticeable in the plots at  $y/D = 4$ ,  $y/D = 7$ , and  $y/D = 10$ , as already seen in Figure 26a.

It is possible that these discrepancies arise from issues in the postprocessing of the k-equation results, as the profiles deviate significantly from the experimental data. This is surprising, considering that the k-equation results align well with experimental trends in other graphs. Moreover, the turbulent inlet profile for the k-equation (Figure 25) is still in close agreement with the experimental data, suggesting that the issue lies not in the model itself but potentially in the postprocessing or specific case setup.

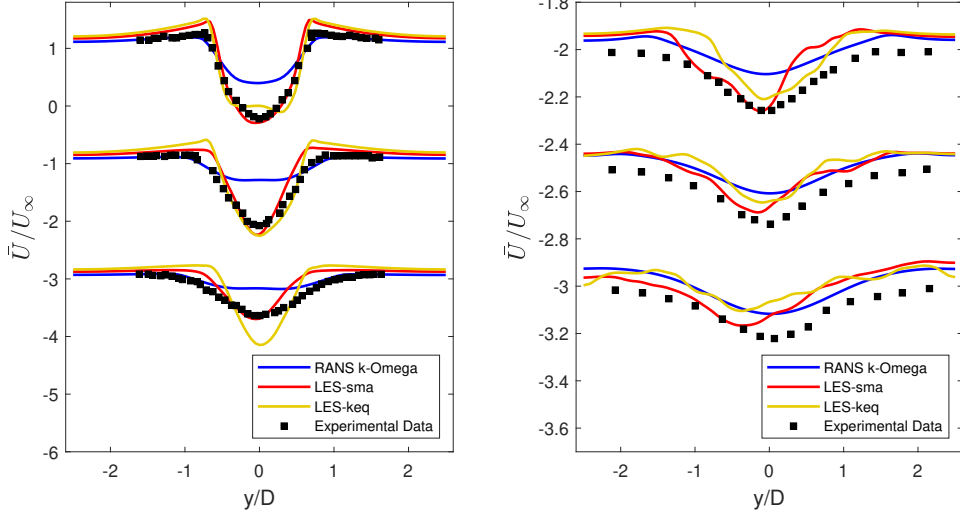


Figure 24: Comparison RANS  $k$ - $\omega$  SST and LES models: Transverse profiles of mean streamwise velocity.  $y$ -axis plotted as in [1]. RANS  $k$ - $\epsilon$  is omitted from the plot for clarity.

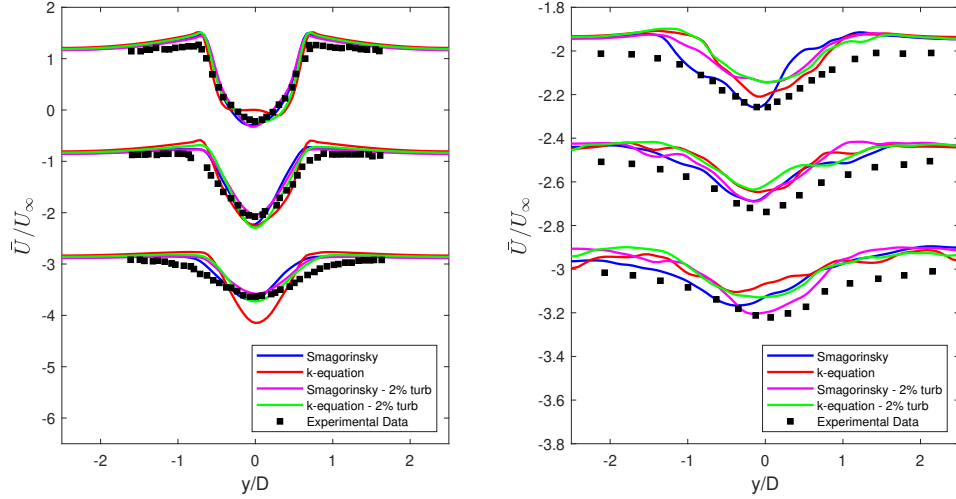
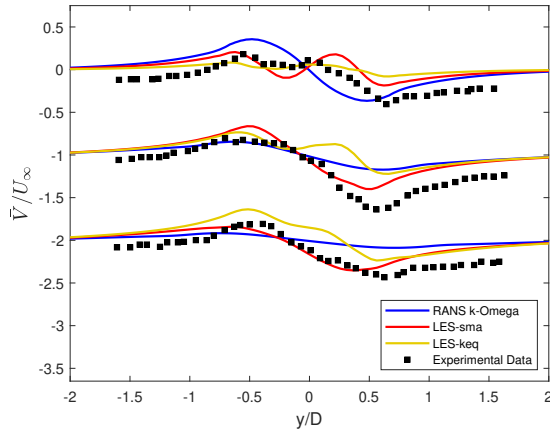
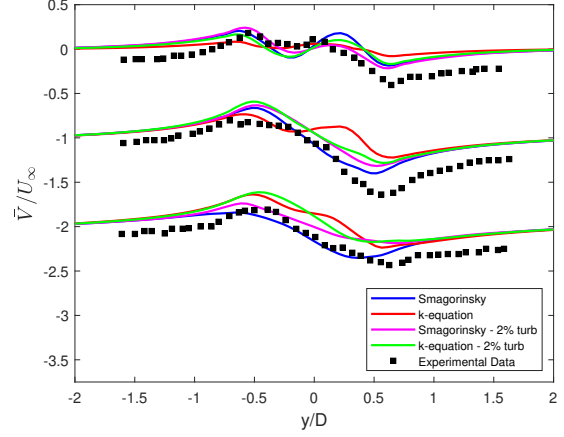


Figure 25: Comparison of LES standard models and LES with 2% turbulence intensity at the inlet: Transverse profiles of mean streamwise velocity.  $y$ -axis plotted as in [1].

The profile of the normalized V component, portrayed in Figure 26, is not correctly captured by the simulations' results. The reason for this discrepancy can be found in the grading applied to the mesh in the y-direction, that reduces the results' quality on this direction. Additionally, the domain size in this axis could be insufficient to correctly capture the velocity behaviour. Furthermore, the referenced study [1] also fails to accurately predict the V-velocity component. Therefore, the obtained results can still be considered reasonably accurate.



(a) Comparison RANS and LES models



(b) Comparison of LES standard models and LES with 2% turbulence intensity at the inlet

Figure 26: Transverse profiles of mean cross-stream velocity.  $y$ -axis plotted as in [1].

### F.2.5. Reynolds stresses

Finally, the Reynolds stresses  $u'^2$  and  $uv$  are analyzed. Similar as before, the LES follows the experimental data the best, but no model is clearly the best. Near the cylinder ( $y/D=1.06$ ) and far from the cylinder ( $y/D \gtrsim 4$ ) the models capture the worst the experimental data profile.

First of all, it can be noticed that the profiles for the LES are not axisymmetrical, while they are for the RANS. It must be recalled that the RANS simulations are longer (stop time = 100 seconds), so the averaged quantity UPrime2Mean is computed over a higher number of periods (22 for the RANS, around 6 for the LES), ensuring its accuracy.

Secondly, the  $uv$  graphs portrayed in Figure 29 and Figure 30 are affected by the same problems along the  $y$ -direction as the Mean velocity component  $V$ , analyzed in Figure 26.

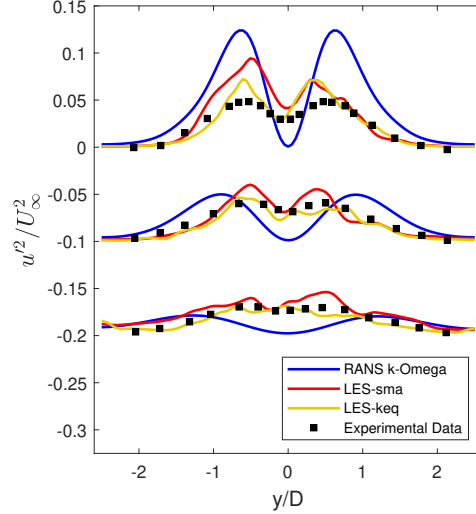
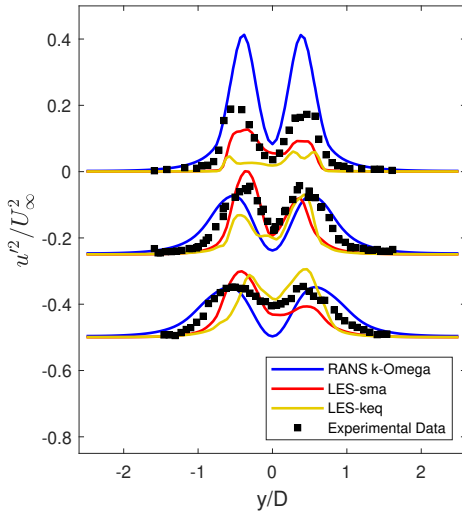


Figure 27: Comparison RANS and LES models: Transverse profiles of the streamwise component of the resolved mean turbulent stress.  $y$ -axis plotted as in [1].

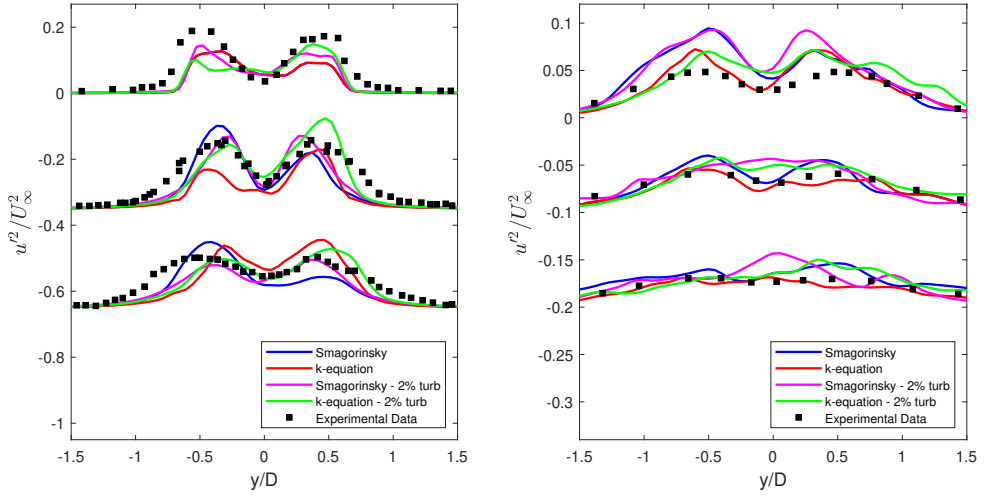


Figure 28: Comparison of LES standard models and LES with 2% turbulence intensity at the inlet; Transverse profiles of the streamwise component of the resolved mean turbulent stress.  $y$ -axis plotted as in [1].

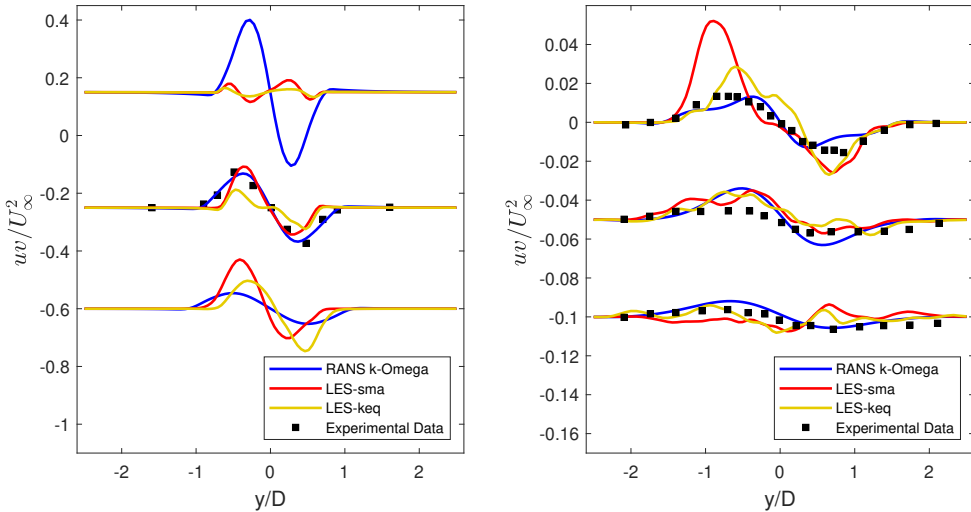


Figure 29: Comparison RANS and LES models; Transverse profiles of mean Reynolds shear stress component.  $y$ -axis plotted as in [1].

## G. Summary and Conclusion

### G.1. Summary

This report analyzes the flow past a cylinder using OpenFoam and various turbulence models: RANS (k-epsilon and k-omega) and LES (Smagorinsky and k-equation). Additionally, a 2% turbulent inlet is added and simulated with the LES methods. The mesh is created by modifying an existing tutorial, and describes the entire flow domain, without relying on any symmetrical property of the domain. Additionally, the quality of the mesh is verified based on the  $y^+$ , Courant number, ratio between resolved kinetic energy and total kinetic energy. Then, RANS and LES results are validated against experimental data.

### G.2. Conclusions

Overall, the proposed results accurately describe the proposed case, achieving a reasonable accuracy with the experimental data. Moreover, some final remarks can be made.

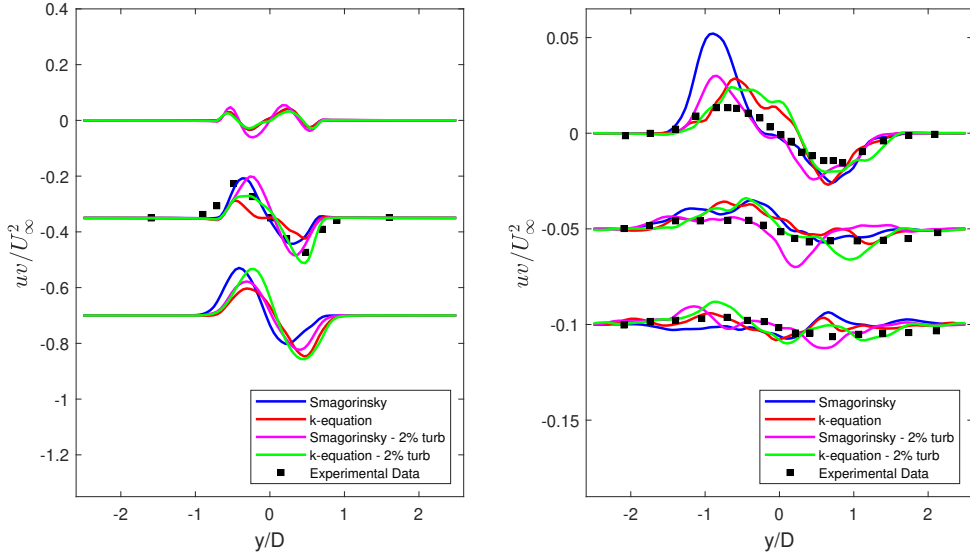


Figure 30: Comparison of LES standard models and LES with 2% turbulence intensity at the inlet; Transverse profiles of mean Reynolds shear stress component.  $y$ -axis plotted as in [1].

### G.2.1. Quality of Mesh

Firstly, the mesh was considered fine enough for RANS simulation and was also good for the LES without turbulent inflow. Adding turbulent inflow increases the small-scale energy and decreases the resolved TKE ratio under the threshold of 80%, hence additional mesh refinement could have been used. Furthermore, the Courant number was sufficiently low in most of the domain, although further mesh refinement can be used close to the cylinder, where the flow speeds up.

### G.2.2. Use of RANS in Turbulence Modeling

Secondly, the RANS simulation using the  $k-\epsilon$  and the  $k-\omega$  SST model have good agreement with experimental results for the pressure coefficient. The skin friction is also close to the LES results outside of the recirculation area. This justifies the use of RANS in some applications, where fast simulations and mean values are more important than accurate knowledge of turbulence quantities in the entire field. RANS can be used best in situations where the local turbulence intensity is low, and no recirculation occurs. Additionally, in general,  $k-\omega$  SST was found to be more accurate than  $k-\epsilon$ , due to its better near wall behaviour.

### G.2.3. Simulation Time for LES cycles

The biggest problem for the LES results can be found in the reduced run time, that allowed for a very small number of vortex shedding oscillation in the fully developed flow. It must also be noted that the LES are significantly computationally heavier than the RANS: in CPU time, running the LES Smagorinsky took 79.76 hours, while running RANS k-Omega SST took 20.01 minutes. Additionally, the LES output is incredibly heavy, and many times the simulations had to be stopped due to disc-memory issues.

### G.2.4. Use of LES in Turbulence Modeling

The LES results were found to be in close agreement with the experimental data for the mean values. For the turbulence properties, the LES has some local errors. The LES k-equation generated more accurate results than the Smagorinsky model and was more robust against the turbulent inflow.

### **G.3. Future work**

To solve some criticalities highlighted above, new LES simulations can be run, with a more refined mesh around the cylinder and longer simulation time, to increase the resolved TKE ratio and achieve better alignment with the experimental results, especially for the Reynold stresses.

## References

- [1] B. N. Rajani, A. Kandasamy, and Sekhar Majumdar. “LES of Flow past Circular Cylinder at  $Re = 3900$ ”. In: *Journal of Applied Fluid Mechanics* 9 (2016). doi: 10.18869/acadpub.jafm.68.228.24178.
- [2] Sharad N. Pachpute. *CFD Modeling of Flow Over a Cylinder*. URL: <https://cfdflowengineering.com/cfd-modeling-of-flow-over-a-cylinder/>.
- [3] Saleh Rezaeiravesh and Mattias Liefvendahl. “Effect of grid resolution on large eddy simulation of wall-bounded turbulence”. In: *Physics of Fluids* 30 (Apr. 2018). doi: 10.1063/1.5025131.
- [4] U. Piomelli. “Large-eddy simulation: achievements and challenges”. In: *Progress in Aerospace Sciences* 35.4 (1999), pp. 335–362. ISSN: 0376-0421. doi: [https://doi.org/10.1016/S0376-0421\(98\)00014-1](https://doi.org/10.1016/S0376-0421(98)00014-1). URL: <https://www.sciencedirect.com/science/article/pii/S0376042198000141>.
- [5] David Wilcox. *Turbulence Modeling for CFD (Hardcover)*. 3rd ed. Jan. 2006.
- [6] Pierre Sagaut and Yu-Tai Lee. “Large Eddy Simulation for Incompressible Flows: An Introduction. Scientific Computation Series”. In: *Applied Mechanics Reviews* 55 (Nov. 2002), pp. 115–. doi: 10.1115/1.1508154.
- [7] Sighard F. Hoerner. *Fluid-Dynamic Drag. Practical Information on Aerodynamic Drag and Hydrodynamic Resistance*. Hoerner Fluid Dynamics, 1965, p. 3.9.